The Effect of AZ61 Content on Mechanical Strength and Surface Hardness of PA6-AZ61 Magnesium Alloy

Yopi Yusuf Tanoto and Song-Jeng Huang[*]

Department of Mechanical Engineering, National Taiwan University of Science and Technology, Taipei 10607, Taiwan

Abstract: In this study, a Polyamide 6 (PA6)-AZ61 magnesium alloy composite and pure PA6 were fabricated using a compression molding instrument. Both the matrix and reinforcement were prepared in powder form. A planetary ball milling machine was employed to mix the PA6 and AZ61 micro powders. The effects of AZ61 content at different percentage on the final properties of the composite were investigated. X-ray diffraction (XRD) analysis and scanning electron microscopy with energy-dispersive X-ray spectroscopy (SEM-EDS) were employed to verify the uniformity of the mixing process and to confirm the composition of both the raw materials and the composite. The result, relative to pristine PA6, the ultimate tensile strength (UTS) demonstrated a substantial increment of 48.3%, reaching 58 MPa. Whereas the yield strength (YS) exhibited a notable surge to 49.38 MPa, constituting a 52.9% enhancement. Additionally, the PA6-5AZ61 composition achieved the highest microhardness value at 21.162 HV, signifying a remarkable 66.3% augmentation compared to the unalloyed PA6 material. This result suggests that AZ61 has the potential to improve the properties of the matrix material.

Keywords: Magnesium alloy, mechanical strength, microhardness, polyamide 6.

1. INTRODUCTION

Polymer matrix composites (PMC) have been employed in a variety of industries and applications, including electrical and electronic components, as well as biomedical implants, household appliances, and automobile parts [1]. Recent advancements in high performance polymer materials are gaining attention as having the potential to transform the materials used in automobiles [2]. Thermoplastic and its composites are utilized in a range of interior and body applications in automobiles, including instrument panels, seat backs, interior door trims, and bumper beams. The thermoplastic polymers in this application are typically polypropylene (PP), polybutylene terephthalate (PBT), polycarbonate, ABS, polyamide 6 (PA6). They were chosen due of their cost effectiveness in comparison to high performance thermoplastics, such as polysulfone, poly ether ether ketone (PEEK) [3]. PA6 is often used when low cost, high mechanical strength, rigid and stable materials are required [4, 5]. PA6 stands as a semi-crystalline thermoplastic polymer that has garnered extensive use within the realm of engineering thermoplastics. Its reputation is well-established for its remarkable processability, impressive tensile characteristics, and its ability to resist abrasion and chemical exposure [6].

Other materials besides polymers used in the automotive field are magnesium alloys because of their good specific strength [7]. Magnesium and its alloys are desirable to modern businesses, owing primarily to their low density in comparison to typical structural metals. Furthermore, these alloys have a high strength-to-weight ratio, which makes them suitable for use in a variety of structural applications in industries such as automobiles, and marine [8-10]. Magnesium alloys, especially the AZ family, have been applied in the automotive sector as brackets for brake and clutch, housings for the transfer case and gearbox, intake manifolds, transmission cases, wheels, trims, and air bag housings [3].

Several researchers have conducted research using magnesium and polymer materials to take advantage of the advantages of these two materials. Magnesium is used as a polymer coating in healthcare to promote compatibility with the human body. PEEK and magnesium in combination has been used in the medical field as a scaffold [11] and as 3D printing of dental and orthopedic implants as well [12]. Magnesium was also introduced in polylactic acid (PLA) to make biodegradable 3D printing filament [13]. Furthermore, most researchers use a polymer as a magnesium coating to increase corrosion resistance. Such as PLA, PEEK, PMMA and others polymer as coating [14-16].

From previous research, Polymer and magnesium gave a big potential to be mixed as a PMC. The PA6-

Mg alloy composite has the potential to be a lightweight material with good mechanical properties. Thus, it can enhance the performance of automotive components that are made from PA. In this research, the effects of different weight percentages AZ61 magnesium alloy powder as the reinforcement to PA6 matrix were investigated.

2. EXPERIMENTAL

2.1. Material

In this study, white color PA6 powder (DuPont), with a particle size of 200mesh, was utilized as the matrix material. The PA6 powder was procured from Shanghai Guangyuan company. For reinforcement, AZ61 magnesium alloy micro powder with a particle size of 100mesh was employed, it was acquired from TIJO material co., Ltd. China was applied for reinforcement [17]. AZ61 was incorporated into the matrix at various weight percentages, specifically 1 wt.%, 3 wt.%, 5 wt.% 10 wt.% and 15 wt.%. The resulting polymeric composites were denoted as PA6-1AZ61, PA6-3AZ61, PA6-5AZ61, PA6-10AZ61 and PA6-15AZ61, respectively.

2.2. Composite Preparation

The blending of PA6 powder and AZ61 powder was carried out using a Retsch PM100 planetary ball milling machine, equipped with 10 mm stainless steel grinding balls. The experimental parameters were set as follows: a milling speed of 300 rpm, a milling duration of 30 minutes, and a ball-to-powder ratio of 1:1, signifying the utilization of an equal weight of stainless-steel grinding balls concerning the combined weight of PA6 and AZ61 powders. After the mixing process, the composite powder was transformed into a composite plate through compression molding. The utilization of compression molding represents a prominent technique employed in the fabrication of polymers and their composites [18, 19]. Both pristine PA6 and the composite powders were preheated to 80 °C, to minimize moisture content, thereby, reducing the presence of air bubbles during the compression molding process [20]. The material and mold were simultaneously heated, with the temperature ranging from 150 °C to 220 °C. This preheating process spanned 10 minutes. Once the temperature reached 220 °C, a low pressure of 3 MPa was applied for 1 minute. Subsequently, the pressure was released to 0 MPa. Following this, a pressure of 7 MPa was applied for 4 minutes. After this step, the mold and material were allowed to cool from 220 °C to 150 °C, a process lasting 40 minutes, while maintaining the same pressure. The pressure was then released, and the mold was removed, permitting it to cool to room temperature before extracting the material. Subsequently, tensile specimens were cut according to ASTM D638 type IV specifications using laser jet cutting.

2.3. Characterization

The morphology of PA6 and AZ61 powder was investigated using a field emission scanning electron microscope (FE-SEM) model JSM-7900 from Jeol Ltd., Japan. This same instrument was also utilized to examine the elemental mapping of the composite powder. It is also used to observe the elemental mapping of the composite powder. The X-ray diffraction (XRD) patterns of both the original materials and the composites were examined using the D2 Phaser instrument from Bruker (Germany). The scanning range (2θ) was set from 10° to 80° with a step size of 0.04° and a scanning rate of 4.8°min-1 for AZ61 powder. For pristine PA6 and the PA6-AZ61 composite, the step size was 0.05° and the scan rate was 10°/min. The tensile test was conducted using the universal tensile testing device, Insight-100 (MTS Systems Corp., USA). Surface properties were observed using a microhardness tester, Wilson HV1102, with an applied pressure of HV 0.1 kgf for a 10-second indentation period.

3. RESULT AND DISCUSSION

3.1. Material Characterization

As seen in Figure **1**, the morphology of PA6 particles is non-spherical, featuring irregular shapes and distinct sharp edges [21]. On the other hand, the AZ61 particles have a spherical shape [22]. The XRD pattern peaks of the matrix, reinforcement, and composite material are visible in Figure **2**. AZ61 exhibits a dominant peak corresponding to the $Mg_{0.97}Zn_{0.03}$ phase, along with some $Al_{12}Mg_{17}$ phase. PA6, being a polymer, shows 2 peaks corresponding to the crystalline phase. The diffraction peaks observed at 20° and 24° in the 2θ angle can be attributed to the reflections corresponding to the (200) and (002, 202) crystallographic planes in the alpha phase of PA6 [23].

The particle morphology and elemental mapping after mixing were also observed using SEM images, as shown in Figure **3**. Figure **3a** display SEM images of
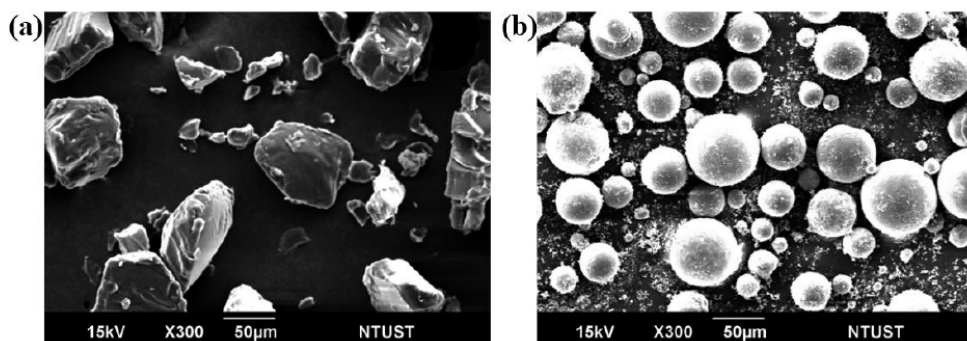
Figure 1: SEM images of (**a**) PA6 and (**b**) AZ61 as received.
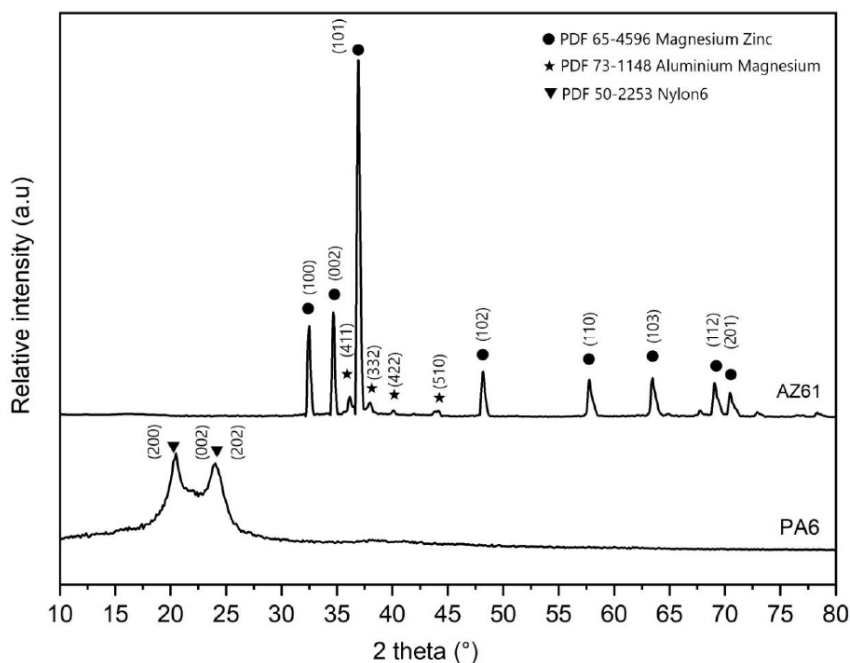
Figure 2: XRD pattern of PA6 and AZ61.

the composite powder with 3 wt.% of reinforcement at magnifications of 500. PA6 consists of carbon (C) elements. While, in AZ61 magnesium alloy, magnesium (Mg) is the predominant element. The AZ61 particles are well-dispersed in the PA6 matrix, as depicted in Figure **3b** and **c**. Magnesium is uniformly distributed on the PA6 particles.

Figure **4** presents the XRD pattern peak of the composite after the completion of the mixing process. Notably, the $Mg_{0.97}Zn_{0.03}$ peak exhibits an increase in intensity, as the quantity of AZ61 rises. In the composite containing 1 weight percent AZ61, the magnesium-zinc peak appears somewhat obscured. However, with the inclusion of 15 weight percent AZ61, the magnesium peak becomes distinctly pronounced. This pattern serves as an indicator of the effectiveness of the blending procedure in achieving a uniform

dispersion of AZ61 throughout the matrix. Nevertheless, it is worth noting that the $Al_{12}Mg_{17}$ peak is not prominently visible in the composite, likely due to its significantly lower content in comparison to the polymer peaks.

3.2. Mechanical and Tribological Properties

The composite material exhibits a higher ultimate tensile strength (UTS) when a moderate quantity of reinforcement is introduced, as compared to pure PA6. The addition of AZ61 in weight percentage leads to a progressive increase in UTS. The UTS of pure PA6 is 39.12 MPa. However, with the addition of 1 and 3 wt.% of AZ61 to PA6, the UTS increases to 48.8 MPa and 58 MPa, respectively. Nonetheless, when the reinforcement content is further increased to 5 wt.%, the UTS decreases to 36.12 MPa. Subsequently, the
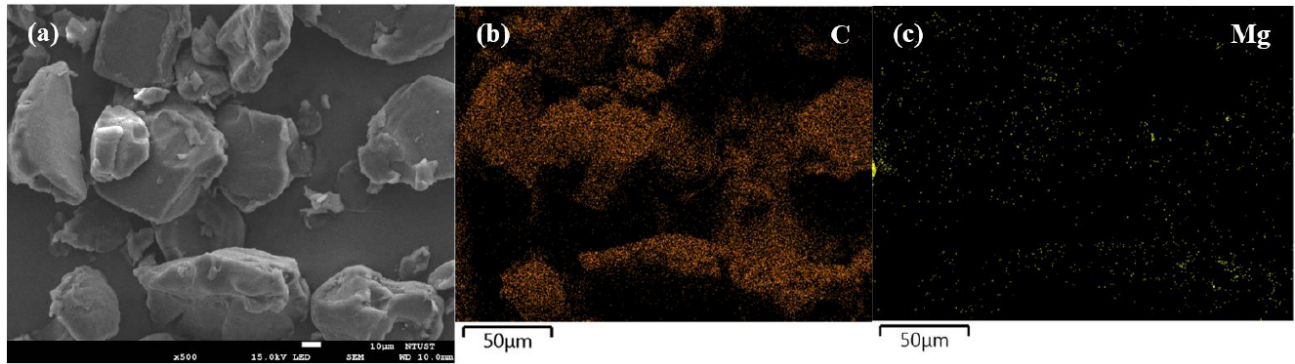
Figure 3: SEM images of PA6-3AZ61 (**a**) 500 magnifications. EDS mapping of (**b**) carbon distribution (**c**) magnesium distribution.
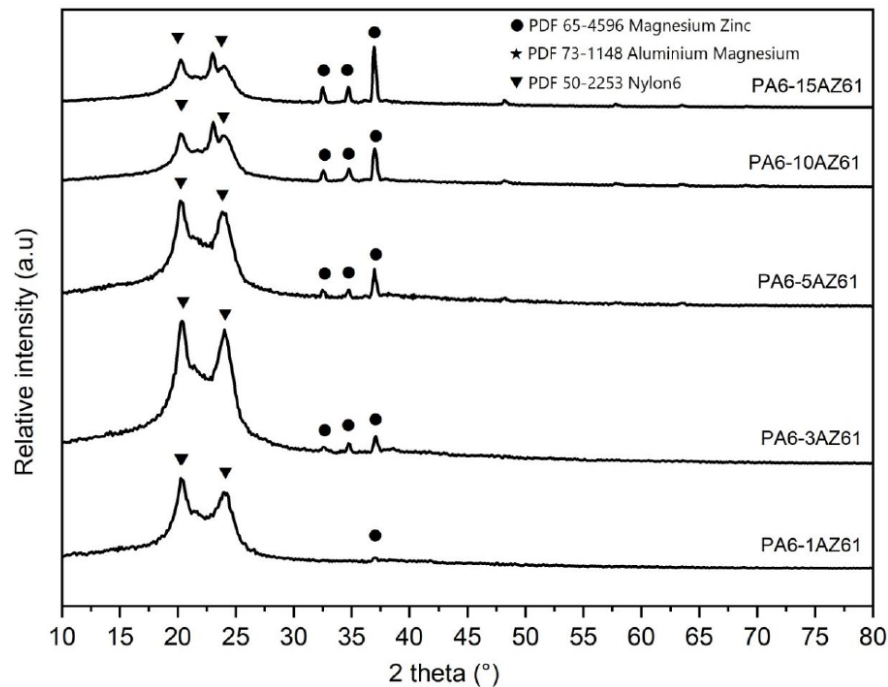
Figure 4: XRD pattern of PA6-AZ61 composite.

UTS stabilizes within the range of 35 to 38 MPa with the introduction of additional reinforcing material. The observed decrease in UTS at higher reinforcement content may be attributed to an increase in stress concentration. Elevated concentration of particle at the interfaces where the particles meet the matrix can lead to heightened stress concentrations. During tensile testing, these stress concentrations have the potential to initiate fractures and propagate, thereby reducing the tensile strength. Although there is a UTS reduction in the case of 5% or higher reinforcement, it is noteworthy that the UTS values remain slightly different from the pristine material.

Both the yield strength (YS) and UTS exhibit similar trends. For the pristine material, the YS measures 32.3 MPa, while for composites with 3 and 5 wt.% reinforcement, it increases to 41.26 MPa and 49.38 MPa, respectively. Nevertheless, the YS decreases with the addition of 5 wt.% reinforcement (31.48 MPa) and remains relatively constant with the introduction of 10 weight percent (33.06 MPa) and 15 weight percent (30.28 MPa) of reinforcement. The tensile strength of both pure PA6 and the PA6-AZ61 composites at various weight percentages is illustrated in Figure **5**.

The microhardness of both pure PA6 and PA6-AZ61 composites at different weight percentages is depicted in Figure **6**. Notably, when compared to pure PA6, the composite materials exhibited higher microhardness values. Furthermore, microhardness showed a gradual increase with a higher percentage of

AZ61 reinforcement. Specifically, the microhardness of pure PA6 was 12.725 HV, and this value increased significantly to 16.55 HV, 19.05 HV, and 21.162 HV with the addition of 1, 3, and 5 weight percent of AZ61, respectively. Interestingly, both PA6-10AZ61 (20.963 HV) and PA6-15AZ61 (20.975 HV) exhibited similar microhardness levels.
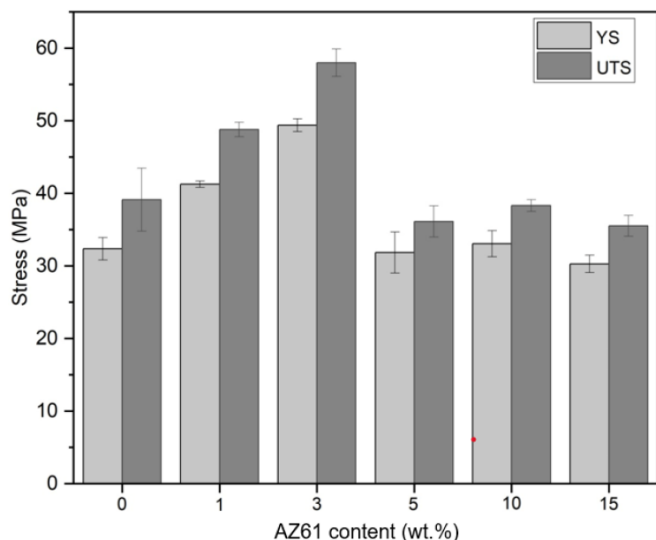
Figure 5: Yield and Ultimate tensile strength for pristine PA6 and the PA6-AZ61 composite.
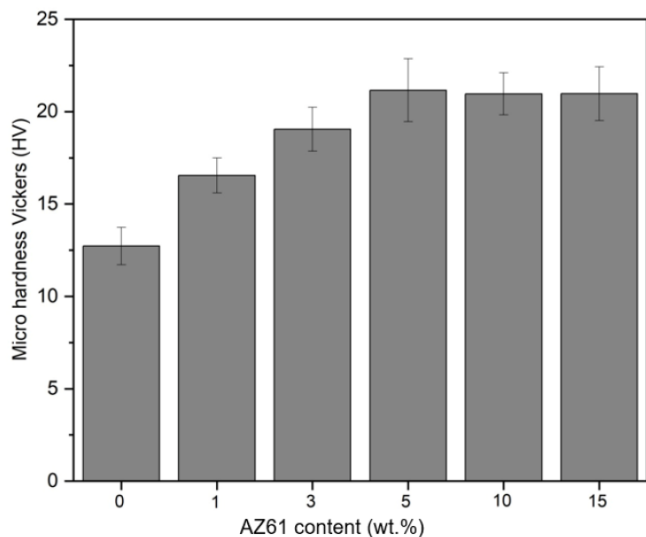
Figure 6: Micro hardness Vickers value for pristine PA6 and the PA6 + AZ61 composite.

4. CONCLUSION

In this research, the impact of incorporating AZ61 reinforcement at various weight percentages was investigated. The investigation involved employing X-ray diffraction (XRD) analysis and scanning electron microscopy with energy-dispersive X-ray spectroscopy

(SEM-EDS) to confirm the uniform and successful distribution of AZ61 particles within the PA6 matrix. The composite material was effectively produced using a compression molding apparatus. Subsequently, the outcomes of the composite samples containing varying AZ61 content were compared to those of pure PA6 specimens, focusing on their tensile strength and microhardness properties.

Notably, the composite with a PA6-3AZ61 composition exhibited exceptional tensile strength results. In comparison to pure PA6, the ultimate tensile strength (UTS) increased by 48.3%, rising from 39.12 MPa to 58 MPa, while the yield strength (YS) increased from 32.3 MPa to 49.38 MPa, representing a 52.9% increase. Furthermore, the PA6-AZ61 composite displayed elevated microhardness values. The highest microhardness value of 21.162 HV was achieved by the PA6-5AZ61 composition, signifying a remarkable 66.3% increase compared to pure PA6. To conclude, the addition of AZ61 particles was found to significantly enhance the tensile and hardness properties of PA6.

DECLARATION OF INTEREST STATEMENT

The authors declare that there is not any conflict of interest with regard to the current study.

ACKNOWLEDGEMENT

REFERENCES

[1]   Hussein AH, *et al*. Graphene-reinforced polymer matrix composites fabricated by in situ shear exfoliation of graphite in polymer solution: processing, rheology, microstructure, and properties. Nanotechnology 2021; 32(17) 175703.
https://doi.org/10.1088/1361-6528/abd359

[2]   Amasawa E, Hasegawa M, Yokokawa N, Sugiyama H, Hirao M. Environmental performance of an electric vehicle composed of 47% polymers and polymer composites. Sustainable Materials and Technologies 2020; 25: e00189.
https://doi.org/10.1016/j.susmat.2020.e00189

[3]   Rowe J. Advanced materials in automotive engineering. Cornwall, UK: Woodhead Publishing 2012.
https://doi.org/10.1533/9780857095466

[4]   Lan P, Nunez EE, Polycarpou AA. Advanced Polymeric Coatings and Their Applications: Green Tribology. In Encyclopedia of Renewable and Sustainable Materials, Elsevier 2020; pp. 345-358.
https://doi.org/10.1016/B978-0-12-803581-8.11466-3

[5]   Patil A, Patel A, Purohit R. An overview of Polymeric Materials for Automotive Applications. Materials Today: Proceedings 2017; 4(2): 3807-3815.
https://doi.org/10.1016/j.matpr.2017.02.278

[6]   Pradeepa KG, Shashidhara GM. Comparative Study on Experimental and Kerner Model Predictions of Viscoelastic Properties of Polyamide 6/ Polyvinyl Alcohol Blends. J Res Updates Polym Sci 2018; 7(1): 14-20.
https://doi.org/10.6000/1929-5995.2018.07.01.3

[7]   Liu B, Yang J, Zhang X, Yang Q, Zhang J, Li X. Development and application of magnesium alloy parts for automotive OEMs: A review. Journal of Magnesium and Alloys 2023; p. S2213956723000099.
https://doi.org/10.1016/j.jma.2022.12.015

[8]   Subramani M, Huang S-J, Borodianskiy K. Effect of SiC Nanoparticles on AZ31 Magnesium Alloy. Materials 2022; 15(3): 1004.
https://doi.org/10.3390/ma15031004

[9]   Subramani M, Huang S-J, Borodianskiy K. Effect of WS2 Nanotubes on the Mechanical and Wear Behaviors of AZ31 Stir Casted Magnesium Metal Matrix Composites. J Compos Sci 2022; 6(7): 182.
https://doi.org/10.3390/jcs6070182

[10]   Catar R, Altun H. Investigation of Stress Corrosion Cracking Behaviour of Mg-Al-Zn Alloys in Different pH Environments by SSRT Method. Open Chemistry 2019; 17(1): 972-979.
https://doi.org/10.1515/chem-2019-0104

[11]   Wei X, *et al*. Magnesium surface-activated 3D printed porous PEEK scaffolds for in vivo osseointegration by promoting angiogenesis and osteogenesis. Bioactive Materials 2023; 20: 16-28.
https://doi.org/10.1016/j.bioactmat.2022.05.011

[12]   Sikder P, *et al*. Bioactive amorphous magnesium phosphate-polyetheretherketone composite filaments for 3D printing. Dental Materials 2020; 36(7): 865-883.
https://doi.org/10.1016/j.dental.2020.04.008

[13]   Pascual-González C, *et al*. Processing and properties of PLA/Mg filaments for 3D printing of scaffolds for biomedical applications. RPJ 2022; 28(5): 884-894.
https://doi.org/10.1108/RPJ-06-2021-0152

[14]   Zhang P, *et al*. Improve the binding force of PEEK coating with Mg surface by femtosecond lasers induced micro/nanostructures. J Mater Sci 2021; 56(23): 13313-13322.
https://doi.org/10.1007/s10853-021-06140-5

[15]   Al-Sherify ZF, Dawood NM, Khulief ZT. Corrosion behavior of AZ31 magnesium alloys coated with PMMA/HA as

biodegradable implants. Materials Today: Proceedings 2022; 61: 1100-1108.
https://doi.org/10.1016/j.matpr.2021.11.057

[16]   Rahimi Roshan N, Hassannejad H, Nouri A. Corrosion and mechanical behaviour of biodegradable PLA-cellulose nanocomposite coating on AZ31 magnesium alloy. Surface Engineering 2021; 37(2): 236-245.
https://doi.org/10.1080/02670844.2020.1776093

[17]   Huang S-J, Mose MP. High-energy ball milling-induced crystallographic structure changes of AZ61-Mg alloy for improved hydrogen storage. Journal of Energy Storage 2023; 68: 107773.
https://doi.org/10.1016/j.est.2023.107773

[18]   Emaldi I, Liauw CM, Potgieter H. Stabilization of Polypropylene for Rotational Molding Applications. J Res Updates Polym Sci 2016; 4(4): 179-187.
https://doi.org/10.6000/1929-5995.2015.04.04.2

[19]   He H, Li K. Study on Flexural Strength and Flexural Failure Modes of Carbon Fiber/Epoxy Resin Composites. J Res Updates Polym Sci 2014; 3(1): 10-15.
https://doi.org/10.6000/1929-5995.2014.03.01.2

[20]   Abdelwahab M, Codou A, Anstey A, Mohanty AK, Misra M. Studies on the dimensional stability and mechanical properties of nanobiocomposites from polyamide 6-filled with biocarbon and nanoclay hybrid systems. Composites Part A: Applied Science and Manufacturing 2020; 129: 105695.
https://doi.org/10.1016/j.compositesa.2019.105695

[21]   Verbelen L, Dadbakhsh S, Van Den Eynde M, Kruth J-P, Goderis B, Van Puyvelde P. Characterization of polyamide powders for determination of laser sintering processability. European Polymer Journal 2016; 75: 163-174.
https://doi.org/10.1016/j.eurpolymj.2015.12.014

[22]   Liu S, *et al*. Influence of laser process parameters on the densification, microstructure, and mechanical properties of a selective laser melted AZ61 magnesium alloy. Journal of Alloys and Compounds 2019; 808: 151160.
https://doi.org/10.1016/j.jallcom.2019.06.261

[23]   Zhang X, Sun L, Chen Y, Yin C, Liu D, Ding E. Flame retarded polyamide-6 composites via in situ polymerization of caprolactam with perylene-3,4,9,10-tetracarboxylic dianhydride. SN Appl Sci 2019; 1(11) 1428.
https://doi.org/10.1007/s42452-019-1505-1